INTERNATIONAL JOURNAL OF HYDROGEN ENERGY 45 (2020) 29379–29394

Available online at www.sciencedirect.com

ScienceDirect

journal homepage: www.elsevier.com/locate/he

Study of the mechanical behavior of paper-type GDL in PEMFC based on microstructure morphology

Zhuo Zhang, Pu He, Yan-Jun Dai, Pu-Hang Jin, Wen-Quan Tao *

Key Laboratory of Thermo-Fluid Science & Engineering of MOE, Xi'an Jiaotong University, Xi'an, Shaanxi, 710049, PR China

HIGHLIGHTS

- The microstructure morphology of compressed GDL is obtained by mechanical simulation.
- The nonlinear GDL compressive curve is determined by fibrous layered structure.
- Porosity, diameter and thickness are key parameters affecting compressibility.
- The average and local porosity distribution vary with compressing pressure.

ARTICLE INFO

Article history:
Received 13 March 2020
Received in revised form
8 July 2020
Accepted 26 July 2020
Available online 27 August 2020

Keywords:
GDL
Microstructure
Contact pairs
Compression
Nonlinearity

ABSTRACT

As the softest part in a proton exchange membrane fuel cell (PEMFC), the gas diffusion layer (GDL) could have a large deformation under assembly pressure imposed by bipolar plate, which would have an impact on the cell performance. So, there is an urgent need to clearly reveal the mechanical behavior of GDL under certain pressure. In this paper, the mechanical behavior of paper-type GDL of PEMFC is studied, considering the complex contact environment in the fibrous layered structure. The microstructure of GDL is reconstructed stochastically, then the stress-strain relationship of GDL is explored from the perspective of solid mechanics by using the finite element method. Based on microstructure morphology, it is found that contact pairs and pore space of microstructure are two key factors determining the nonlinearity of the compressive curve. The equivalent Young's modulus increases with the decrease of porosity and carbon fiber diameter but it is not very sensitive to the carbon paper thickness. The results indicate that with the increase in acting pressure, the average porosity of the carbon paper decreases, and the nonuniformity of porosity along the through-plane direction increases. Furthermore, a reasonable explanation for the increase of concentration loss and the decrease of ohmic loss is given from the microstructure findings of the present study.

Introduction

With the advantage of quiet operation process, quick start-up and load response, and efficient energy conversion, polymer electrolyte membrane fuel cell (PEMFC) has become a promising alternative power source for stationary, portable, and vehicular applications [1]. Many fundamental studies have been done to solve the existing challenges against the wider

* *Corresponding author.*
E-mail address: wqtao@mail.xjtu.edu.cn (W.-Q. Tao).
https://doi.org/10.1016/j.ijhydene.2020.07.240

Nomenclature

D	Diffusivity (m^2/s)
E	Young's modulus (Pa)
e	Auxiliary variable
F	Body force (N)
G	Shear elastic modulus (Pa)
s	Standard deviation
x	x direction
y	y direction
z	z direction

Greek letters

γ	Shear strain
ε	Normal strain
λ	Lame constant
ν	Poisson ratio
σ	Normal stress (Pa)
τ	Shear stress (Pa)
φ	Porosity

Subscripts and superscripts

eff	Effective
i	Initial state
l	Local value
j	jth Components

commercialization of PEMFC, which includes cost, performance, and durability [2]. A typical membrane electrode assembly (MEA) of PEMFC is a five-layer structure, including a proton exchange membrane, two catalyst layers (CLs), and two gas diffusion layers (GDLs) sandwiched between two bipolar plates (BPPs) [3]. Among the major components of PEMFC, the gas diffusion layer (GDL), situated between the catalyst layer and bipolar plate, plays multiple roles during the cell operation, such as: (i) transporting the reactant gas into the catalyst layer; (ii) removing the liquid water from the catalyst layer to the gas channel; and (iii) conducting electrons with low resistance. Better design and understanding of GDL's characteristics are critical to improving the performance and durability of PEMFC.

The GDL is a typical porous medium, usually consisting of carbon fiber, polytetrafluoroethylene (PTFE), and binder [4]. In terms of the fiber microstructure, three kinds of commercial GDLs are available on the market, including carbon paper, carbon cloth, and carbon felt [5]. As shown in Fig. 1, the carbon fibers are distributed in a matrix (paper), woven (cloth) structure, and hydro-entangled (felt) in these GDLs, respectively [6]. Each type of them has its own characteristics [3,4,7] and finds its applications in PEMFC practice.

To reduce the thermal and contact resistance inside the PEMFC and also to maintain its seal characteristic, the MEA layer is compressed between the bipolar plates by an initial normal pressure applied during the assembly process [8]. When subjected to such compressive loadings, the GDL deforms considerably, due to its low Young's modulus compared with the CL and BPP. The compressed GDL and pristine GDL are quite different in thickness, porosity, permeability, conductivity, and contact resistance [9], and all these changes will have a profound effect on the cell performance. For example, the GDL compression ratio changing from 14% to 45% will reduce the maximum electrical current from about 1.4 A/cm^2 to 1.0 A/cm^2 [10]. So, there is an urgent need to clearly reveal the mechanical behavior of GDL under certain pressure, which is the basis for the study of other parameters influenced by compression.

Several experiment techniques have been developed to study the compressive behavior of GDL. The following is a brief review in this regard. Using a commercially available cell assembly compression test or any other tensile-compression apparatus, a compression test can be done on a specific GDL. From the experiment results in Refs. [6,11–18], we can find the nonlinear stress-strain curve of compressed GDL. Some researchers used the SEM or the digital microscope to study the microstructure of different kinds of compressed GDL [6,11,13,15,17–21]. From the SEM micrograph, more compact fiber distribution can be observed with an increasing steady load [6], and the bending of carbon fiber occurs obviously, especially in a cross-sectional view [16]. Some authors [6,13,15–17,20,22] measured the bulk resistance, pore size distribution, gas permeability, etc. of the GDL sample as a function of compression pressure. Some researchers considered the effect of cyclic pressure on the deformation of GDL [6,12,13,17] during the compression test. Carral et al. [12] proposed a stress-density constitutive law to consider mechanical history's effect. In addition to studying the GDL sample itself, Nitta [16] and Radhakrishnan et al. [20] considered both the BPP and GDL in the compression test, as it is assembled in practice, and established the relationship between the electric contact resistance and compression pressure. Considering the periodic structure on the bipolar plate, the clamping pressure applied on the GDL is highly uneven. This uneven pressure distribution results in inhomogeneous compression of GDL. The region under the rib may undergo a significant strain, while the region under the channel may intrude into channel [11,16,19,20]. Bazylak et al. [21] utilized fluorescence microscopy to visualize liquid water transport through the cross-plane of a GDL sample. Froning et al. [23] used synchrotron X-ray tomography to get the compressed microstructure and then calculated the gas transport in nonwoven GDLs of a PEMFC with the lattice Boltzmann method.

These experimental methods provide valuable data and visualization of GDL's microstructure, but they are costly and time-consuming. Numerical methods provide an important cost-effective way for such study. The finite element method (FEM) is a common numerical technique to compute the deformation in solid materials. There are many references using FEM simulation to study the deformation of GDL under the BPP. Zhou et al. [24] got the distribution of the gas diffusion layer characteristics (relations between geometry structure, thickness, porosity, and permeability) under the different assembly forces through a 2D FEM simulation. Carral et al. [25] investigated the influence of the assembly phase of PEMFC stacks on the mechanical state of the MEA by a 3-D FEM analysis. Chien et al. [26] studied the effects of bolt pre-loading variations on the performance of GDL, like porosity, resistance, etc. in a bolted PEMFC stacks by a 3-D FEM analysis. Peng et al. [27] investigated the influences of coating, weld,

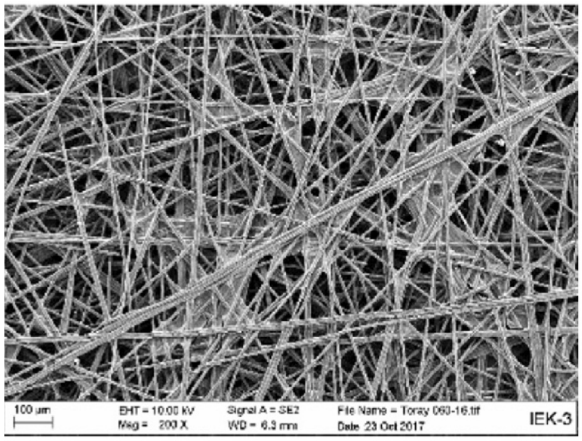

(a) Carbon paper

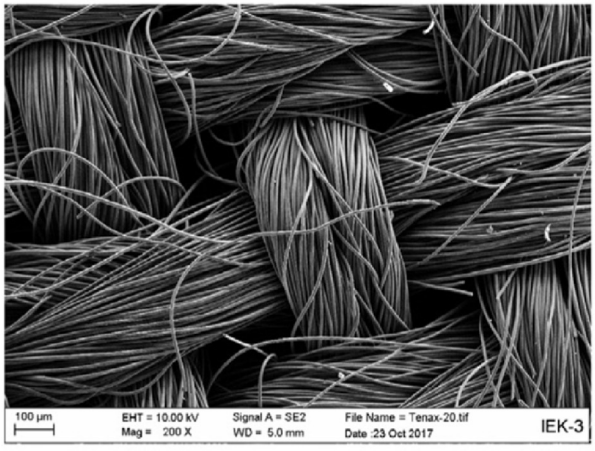

(b) Carbon cloth

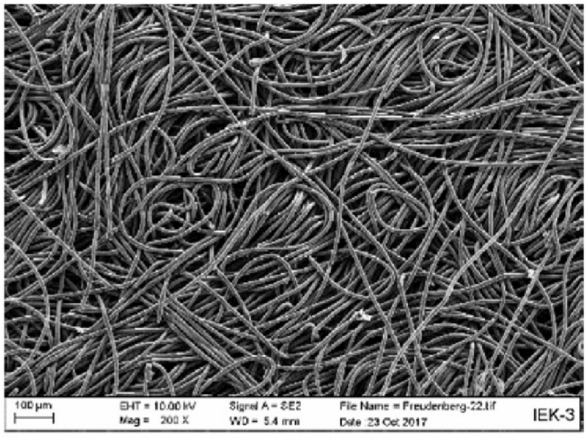

(c) Carbon felt

Fig. 1 – SEM image of carbon paper, carbon cloth and carbon felt [6].

and dimensional error on the contact resistance through a FEM model of BPP/GDL assembly. Many researchers coupled the FEM mechanical analysis and computational fluid dynamics (CFD) simulation to study the cell performance under different assembly pressure. In this method, the compressed GDL's characters predicted by the FEM, like porosity, diffusivity, and conductivity, are incorporated into 3-D [11,24,30–35] or 2-D [28,29] models of a PEMFC or a stack. In this kind of FEM simulation, there are two practices in dealing with GDL mechanical properties. A simple practice is regarding GDL from a macroscopic view and taking it as an isotropic material. Then Young's modulus of GDL domain is a key value that determines the simulation result. Even though carbon paper GDL has a relatively high modulus in its in-plane direction compared with that in its through-plane direction, some scholars still regarded the carbon paper as an isotropic material and set a constant Young's modulus in the GDL domain. For example, in Refs. [24,27,32–34], Young's modulus of GDL is set as 6.3 MPa, and in Ref. [8] as 10 MPa. A more reasonable practice is to take its anisotropic character into consideration. In this regard, Lu et al. [36] took in-plane modulus $E_x = E_y = 1500$ MPa, and $E_z = 9$ MPa in an orthotropic model. To further establish a more accurate model, the nonlinear character of through-plane Young's modulus E_z should be considered. Kleemann et al. [37] tested some commercial GDL materials and recorded the nonlinear, declining compression behavior in through-plane direction. Their results show a pronounced material hardening at high strains. Based on their test data, the dependency $E_z = f(\varepsilon_z)$ was expressed using a polynomial fit function for each GDL and used as an input for the structural simulation. Refs [25,31,36–40] all used this method to describe the GDL's through-plane direction Young's modulus. One weak point of such numerical study is that the macroscopic method supposes the deformation of GDL is homogeneous, which does not conform to actual situation. In addition, such macroscopic study is unable to capture local morphology change of microstructure in GDL.

According to the SEM image, paper-based carbon fiber GDLs can be regarded as a thin layer of stacked cylinders that extend far more into the in-plane direction than the through-plane direction. If we can study the GDL's deformation based on its real microstructure, then the characteristics and essence of it could be revealed more deeply. Some researchers [8,41,42] used an analytic method to predict the compressive behavior of GDL, based on the simplified geometry. In their model, some key parameters still need to be obtained from experimental results. Toll et al. [43] studied the process of fiber packing and a micromechanical theory based on the contact points statistics was developed for the forced packing. It reveals that the applied pressure will be a nonlinear function of fiber volume fraction. As for the numerical methods, discrete element method (DEM) is a special way to simulate the movement of granular materials through a series of calculations that trace individual particles constituting the granular material. Rodney et al. [44] used this method to study the entanglement transition of non-cross-linked semi-flexible fibers during isostatic compressions. Then Barbier et al. [45] extended the previous discrete element model [44] to study the influence of static friction on the mechanical response of assemblies. Besides DEM, the FEM analysis was carried out by Sui et al. [46] and Jiao et al. [47,48] recently, based on a stochastic microstructure model. Then the two-phase flow of water and diffusion of reaction gas was investigated in the compressed GDL.

From the above brief review, it can be seen that in the numerical methods for studying the compression behavior of GDL, there is still a large room for improvement. From the macroscopic point view, FEM is a good simulation method for mechanical problems, but usually, in this method, Young's modulus in the through-plane direction of GDL is represented by an empirical nonlinear stress-strain relationship through curve fitting of experimental data. Hence, it cannot reveal the dependence of mechanical behavior as a function of the GDL microstructure. On the other hand, from the microscopic view, although the research using the DEM method or FEM method could get the compressed microstructure of GDL, there is a lack of analysis of the nonlinear mechanical behavior of carbon paper combined with the microstructure morphology. Moreover, the effect of key parameters (porosity, carbon fiber diameter, and thickness) of carbon paper on its mechanical characteristics should also be addressed based on the microstructure view.

This paper numerically studies the GDL compression behavior based on its microstructure. As indicated above, there are three types of GDL, and each type has its own characteristics. Among them, carbon paper is regarded as one of the most promising candidates for the use of its high porosity and good electricity conductivity [4,7]. In addition, for the microstructure study, a stochastic reconstruction method is very important. Among the three types of GDL, it is the carbon paper that such a method has been well developed [49–57]. Thus, the present study works on carbon paper. In our study, the microstructure of carbon paper is stochastically reconstructed, and the FEM is applied to perform the solid mechanical simulation. The nonlinear stress-strain law of typical carbon paper is obtained from the simulation results, which is in good agreement with the experimental data. By analyzing the deformed morphology of carbon paper, the mechanism of deformation has been revealed. Then three key parameters, porosity, carbon fiber diameter, and thickness, are studied from a microscopic view. How these three factors affect the stress-strain law of carbon paper is also analyzed. Furthermore, from the compression results, the effect of compression on GDL's porosity distribution and cell performance is discussed.

The rest of the paper is organized as follows. Section Model description describes physical and numerical models, including the governing equations, boundary conditions, and numerical procedures. Section Result and discussion presents numerical results and discussion. Finally, some conclusions are drawn in Section Conclusions.

Model description

Model assumptions and construction of fiber matrix

The stochastic algorithm for construction of fiber matrix we employed here has been widely used in numerical simulation

of GDL region [49–55], and it is based on the following assumptions:

(1) Carbon fibers are straight cylinders with a constant diameter, and they are placed in the x-y plane randomly [49,56]. The overlap of the fibers in a layer is allowed.
(2) The component of PTFE and binder inside the carbon paper are ignored, and the bonded contact constraint is used to replace their role, which is a popular assumption adopted in Refs. [46,48].
(3) The carbon fiber is initially homogeneous in the through-plane direction, which means each layer has the same given porosity.
(4) Only the elastic deformation of carbon fiber is considered, and plastic deformation or damage of carbon fiber under stress is neglected.
(5) The Young's modulus of fibers has been treated as isotropic [46–48], and it is set as the transverse Young's modulus of carbon fiber [47].

About the 5th assumption, 3 Young's modulus values, 3 GPa (transverse Young's modulus of carbon fiber), 10 GPa, and 200 GPa (longitudinal Young's modulus carbon fiber) have been tested. Finally, we have found that 3 GPa could best characterize the carbon paper's equivalent mechanical behavior.

The computational domain is set up as follows, the in-plane (x-y plane) area is fixed at 120 μm × 120 μm, while the through-plane distance or the thickness of carbon paper depends on the layer numbers and carbon diameter, which will be given in advance for each simulation case. As for the in-plane area of the computation domain, too small or too big, are both inappropriate. It should be balanced between result accuracy and time efficiency. In the present study, we compare the carbon paper's compression value under the pressure of 2.5 MPa for three cases with different size of the in-plane area: 120 μm × 120 μm, 180 μm × 180 μm, and 240 μm × 240 μm, and the differences among them are listed in Table 1. It can be seen that the size 120 μm × 120 μm is large enough, so 120 μm × 120 μm is chosen as the in-plane area of 120 μm × 120 μm. To simulate the working condition of the rear GDL, which is sandwiched between the BBP and CL, and to apply the boundary condition easier, two plates at both ends of the computational domain are placed.

The workflow of constructing a computational model is shown in Fig. 2. It's worth pointing out that the first step, generating a cylinder in the Nth layer, consists of complicated Boolean operation to truncate the fiber volume to the size of a finite space. To execute the whole workflow, the ANSYS Parametric Design Language, a scripting language, is used to build the model in terms of parameters. Fig. 3 shows a model constructed by this method.

Table 1 – The plate displacement and strain value in three cases.

	120 μm × 120 μm	180 μm × 180 μm	240 μm × 240 μm
Displacement of stressed plate/μm	63.23	62.93	63.41
Strain	0.224	0.223	0.224

Governing equations and boundary conditions

The elastic deformation of the GDL under certain pressure is modeled using the elastic mechanics of material, which is governed by the equilibrium, geometric, and constitutive equations, as listed in Eqs. (1)–(6).

(1) Equilibrium equations:

$$\begin{cases} \frac{\partial \sigma_x}{\partial x}+\frac{\partial \tau_{xy}}{\partial y}+\frac{\partial \tau_{xz}}{\partial z}+F_x=0 \\ \frac{\partial \sigma_y}{\partial y}+\frac{\partial \tau_{yx}}{\partial x}+\frac{\partial \tau_{yz}}{\partial z}+F_y=0 \\ \frac{\partial \sigma_z}{\partial z}+\frac{\partial \tau_{zx}}{\partial x}+\frac{\partial \tau_{zy}}{\partial y}+F_z=0 \end{cases} \tag{1}$$

(2) Geometric equations:

$$\begin{cases} \frac{\partial^2 \varepsilon_x}{\partial y^2}+\frac{\partial^2 \varepsilon_y}{\partial x^2}-\frac{\partial^2 \gamma_{xy}}{\partial x \partial y}=0 \\ \frac{\partial^2 \varepsilon_y}{\partial z^2}+\frac{\partial^2 \varepsilon_z}{\partial y^2}-\frac{\partial^2 \gamma_{yz}}{\partial y \partial z}=0 \\ \frac{\partial^2 \varepsilon_z}{\partial x^2}+\frac{\partial^2 \varepsilon_x}{\partial z^2}-\frac{\partial^2 \gamma_{zx}}{\partial z \partial x}=0 \\ \frac{\partial}{\partial x}\left(\frac{\partial \gamma_{xy}}{\partial z}+\frac{\partial \gamma_{xz}}{\partial y}-\frac{\partial \gamma_{yz}}{\partial x}\right)-2\frac{\partial^2 \varepsilon_x}{\partial y \partial z}=0 \\ \frac{\partial}{\partial y}\left(\frac{\partial \gamma_{yx}}{\partial z}+\frac{\partial \gamma_{yz}}{\partial x}-\frac{\partial \gamma_{xz}}{\partial y}\right)-2\frac{\partial^2 \varepsilon_y}{\partial x \partial z}=0 \\ \frac{\partial}{\partial z}\left(\frac{\partial \gamma_{zx}}{\partial y}+\frac{\partial \gamma_{zy}}{\partial x}-\frac{\partial \gamma_{xy}}{\partial z}\right)-2\frac{\partial^2 \varepsilon_z}{\partial x \partial y}=0 \end{cases} \tag{2}$$

(3) Constitutive equations:

$$\begin{cases} \sigma_x=\lambda e+2G\varepsilon_x \\ \sigma_y=\lambda e+2G\varepsilon_y \\ \sigma_z=\lambda e+2G\varepsilon_z \\ \gamma_{xy}=\frac{\tau_{xy}}{G} \\ \gamma_{xz}=\frac{\tau_{xz}}{G} \\ \gamma_{yz}=\frac{\tau_{yz}}{G} \end{cases} \tag{3}$$

In the above equations,

$$e=\varepsilon_x+\varepsilon_y+\varepsilon_z \tag{4}$$

$$\lambda=\frac{\nu E}{(1+\nu)(1-2\nu)} \tag{5}$$

$$G=\frac{E}{2(1+\nu)} \tag{6}$$

The Young's modulus and Poisson ratio adopted in this paper are listed in Table 2. Because we only consider the GDL's deformation, Young's modulus of the two endplates is set to a big value enabling them be treated as rigid body.

Table 3 lists boundary condition settings in the model (see Fig. 3(b)).

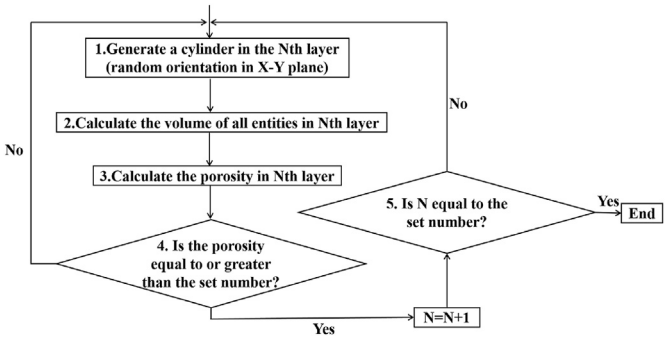

Fig. 2 – Flow chart of reconstruction.

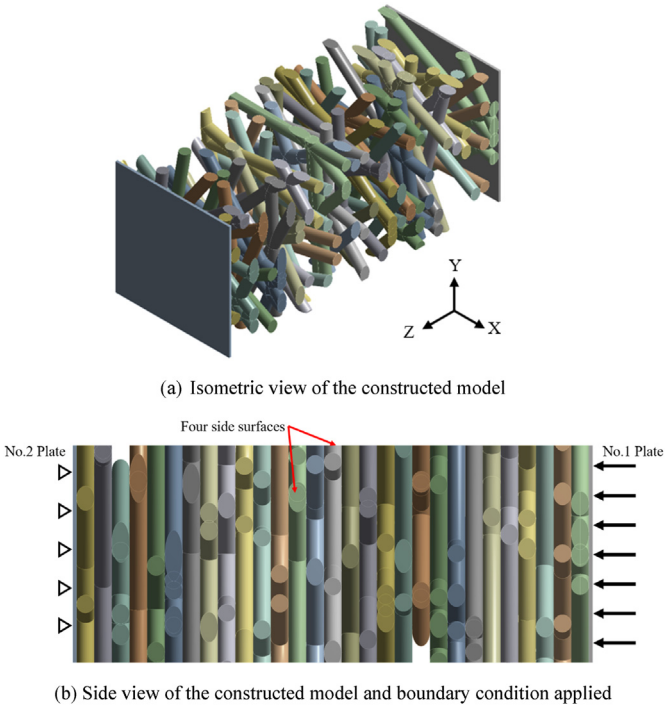

(a) Isometric view of the constructed model

(b) Side view of the constructed model and boundary condition applied

Fig. 3 – Example of the constructed model.

Table 2 – Physical property of plate and carbon fiber [47,58].

	Fiber	Endplate
Young's modulus (GPa)	3	13
Poisson ratio	0.256	0.26

Table 3 – Boundary condition list.

Boundary	Conditions
No.1 Plate (one side)	Pressure
No.2 Plate (one side)	Fixed support
Four side surfaces	Symmetry

To improve the convergence of calculation, the load of 2.5 MPa is applied in twelve steps. In the first four load steps, the pressure increment is 0.125 MPa, while in the last eight load steps, it is 0.25 MPa. For each load step after getting the converged solution, the next load step computation begins.

Contact settings between fibers

Besides the boundary condition settings of the endplates and the surrounding areas, the contact type for the complex contacting pairs existing inside the model is also necessary to be specified. In the GDL microstructure, carbon fibers of adjacent layers are bonded by the PTFE, and as described in subsection Model assumptions and construction of fiber matrix, they are set to be "Bond" contact type. That means these contacting pairs initially contact each other. After the force is applied,

they will not be separated or slide. However, for those surfaces of carbon fibers that do not contact initially, contact may occur during the load increase process. After each load increment, the newly contacting surfaces will be iteratively detected, and this contact type is set as "contact-after-compression (CAC)". Our contact detection algorithm can ensure that those fibers not initially contacting may become contacting in the subsequent appropriate load increment, rather than penetrating with each other.

The Bond type contacts are given as initial condition, while CAC type contacts are nonlinear in that they are detected in the pressing process gradually, and their determination requires multiple equilibrium iterations to obtain the convergence solution. It should be mentioned that if only adopting the bond contact type, which is set at initial stage and omitting the CAC type contact, the nonlinear deformation characteristics during deformation of carbon paper cannot be reflected in the stress-strain curve, as can be seen in the later discussion of model validation.

Numerical procedure

Even though the computational domain is a simple cubic space, it includes many small fibers that are randomly positioned. Thus, the unstructured mesh was adopted to discretize the computational domain. We perform the grid independence analysis with five different grid numbers: 289,616, 571,715, 723,794, 798,258, 1,164,885, as shown in Fig. 4. The maximum deformation value of the whole computational domain approximately does not change until the node number reaches 0.79 million. Considering the accuracy, computer source, and time limit, we adopted a grid number of 0.8 million here to perform the numerical simulation. A typical example of the constructed grids is shown in Fig. 5. Because the curvature size function controls the generation of unstructured grids, so the different section shapes exhibit different mesh density. And the different section shapes are caused by the random orientation of fibers, and the truncation during the reconstruction process. The mechanical model was solved by the commercial software ANSYS Workbench 17.2. Distributed memory sparse direct solution was adopted to solve the governing equation. Table 4 lists the cases studied in this paper.

Result and discussion

In this section, firstly, the model we constructed is validated with experimental data. Then, the nonlinear deformation behavior of carbon paper is discussed from the point of view of the microstructure in detail. After that, the effects of porosity, fiber diameter, and thickness on carbon paper's deformation are analyzed. Seven cases with different parameters are analyzed in detail. Finally, the effects of compression on average and local porosity are presented.

Model validation

To validate the proposed numerical model, the predicted compression curve for the TGP-H-90 GDL sample is compared with the experimental data reported by Mathias et al. [4]. The major parameters of TGP-H-090 are listed in Case 1 of Table 4. Here, stress denotes the pressure applied on the plate, and the strain value is calculated by plate displacement divided by the carbon paper's original thickness. As shown in Fig. 6, the predicted compressive curve of Bond and CAC contact setting is generally in good agreement with the experimental data. For comparison, the result of only Bond contact setting is also presented in the figure. It shows a linear stress-strain curve which cannot reflect the carbon paper's nonlinear mechanical behavior during compression. Fundamentally, this nonlinear character of deformation is caused by the complex microstructure, which we will analyze from a microscopic view later.

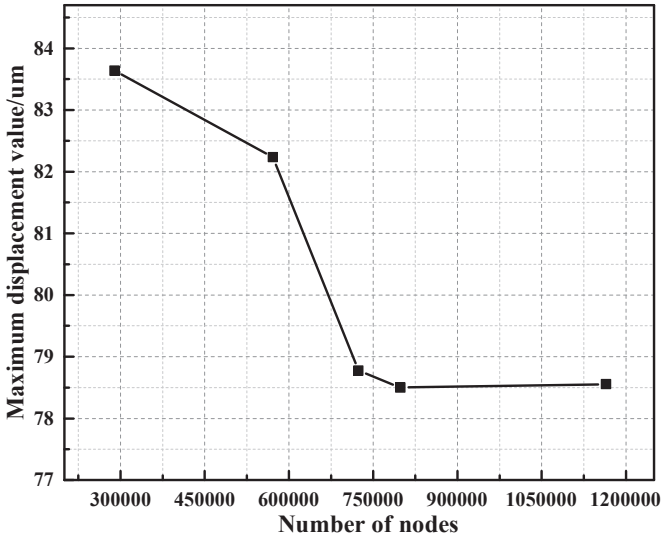

Fig. 4 – Grid independence examination.

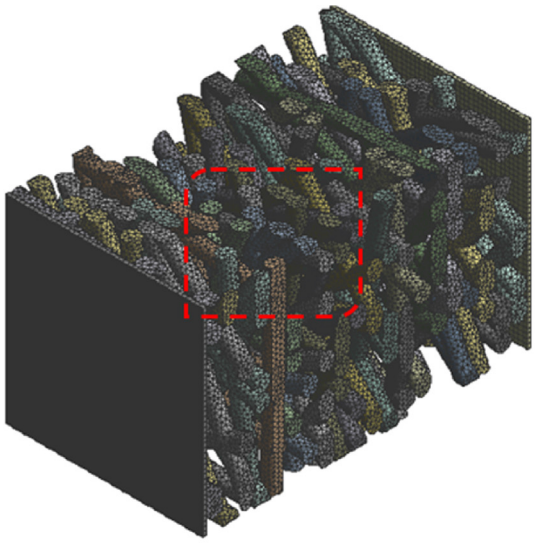

(a) Example of unstructured grid

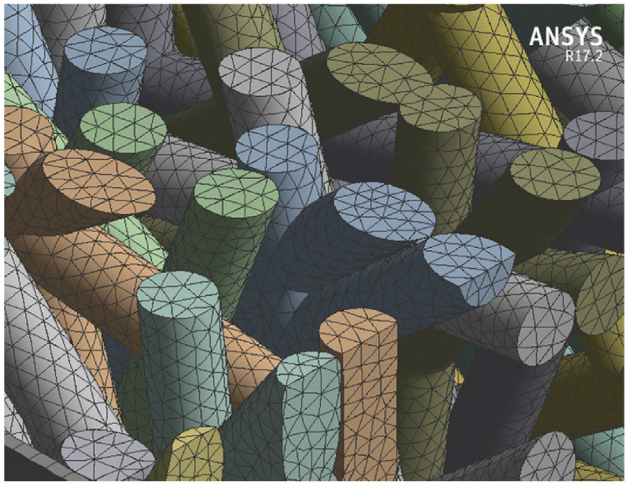

(b) Local enlarged picture

Fig. 5 – Example of the unstructured grid system.

Table 4 – Parameters of different cases.

Carbon paper type	Case number	Porosity	Fiber diameter/μm	Thickness/μm
TGP-H-090	Case 1	78%	9.75	282.75
TGP-H-060	Case 2	58%	9.75	195
	Case 3	68%	9.75	195
	Case 4	73%	9.75	195
	Case 5	78%	9.75	195
	Case 6	78%	8	192
TGP-H-120	Case 7	78%	9.75	370.5

Nonlinearity analysis

Nonlinear deformation

The nonlinear deformation of carbon paper is fundamentally caused by its microstructure. Shown in Figs. 7(a)–(e) are the deformed carbon paper microstructure of Case 1 under the pressure of 0.5 MPa, 1 MPa, 1.5 MPa, 2 MPa, and 2.5 MPa respectively. In order to better observe the changes of the internal microstructure, the section view of the middle section in the x direction is given in addition to the isometric and side views (shown the side by a thick arrow in an isometric figure). The location of the section can be found in the isometric picture under each pressure.

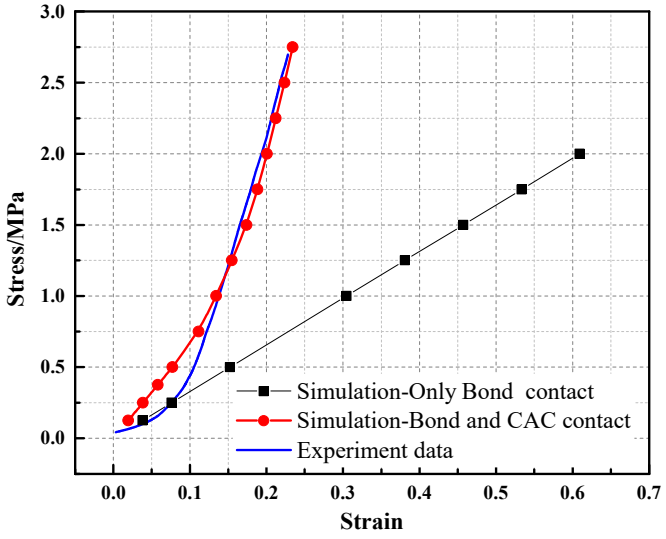

Fig. 6 – Model validation.

From Figs. 7(a)–(e), it can be observed that, with the increase of applied pressure, the degree of extrusion deformation of carbon paper increases gradually. After the carbon paper is compressed, the structure becomes closer, which is consistent with the phenomenon observed in the experiment [6]. From the side view and section view, the bending deformation of carbon fiber can be observed. The original pore space will be occupied by the bent carbon fiber. And the originally separated carbon fibers may contact after being compressed [17]. The contact process of the carbon fibers in the red frame in the figure is a typical example. The two fibers in the red frame initially are separated, and when the pressure reaches 1.5 MPa, one of them is bent more appreciably, and they come into contact.

By observing the position of the stressed plate after each increment of compression force, it can be found that with the increase of pressure, the compression of carbon paper becomes more and more difficult, which is consistent with the compressive curve in Fig. 6. When the stress of carbon paper is small, the deformation extent is small. There exist more pores and fewer contact pairs between fibers. For particular carbon fiber, it is more prone to deform when it encounters pores than when it encounters another carbon fiber, which can hinder its bending. Therefore, the resistance of carbon fiber against bending is small when the stress of carbon paper is small. With the increase of stress, more pores in carbon paper have been occupied by the bent carbon fiber because of the increasing deformation extent of carbon paper. At the same time, there are more carbon fiber contact points in the inner part of carbon paper, which can transfer the force to each

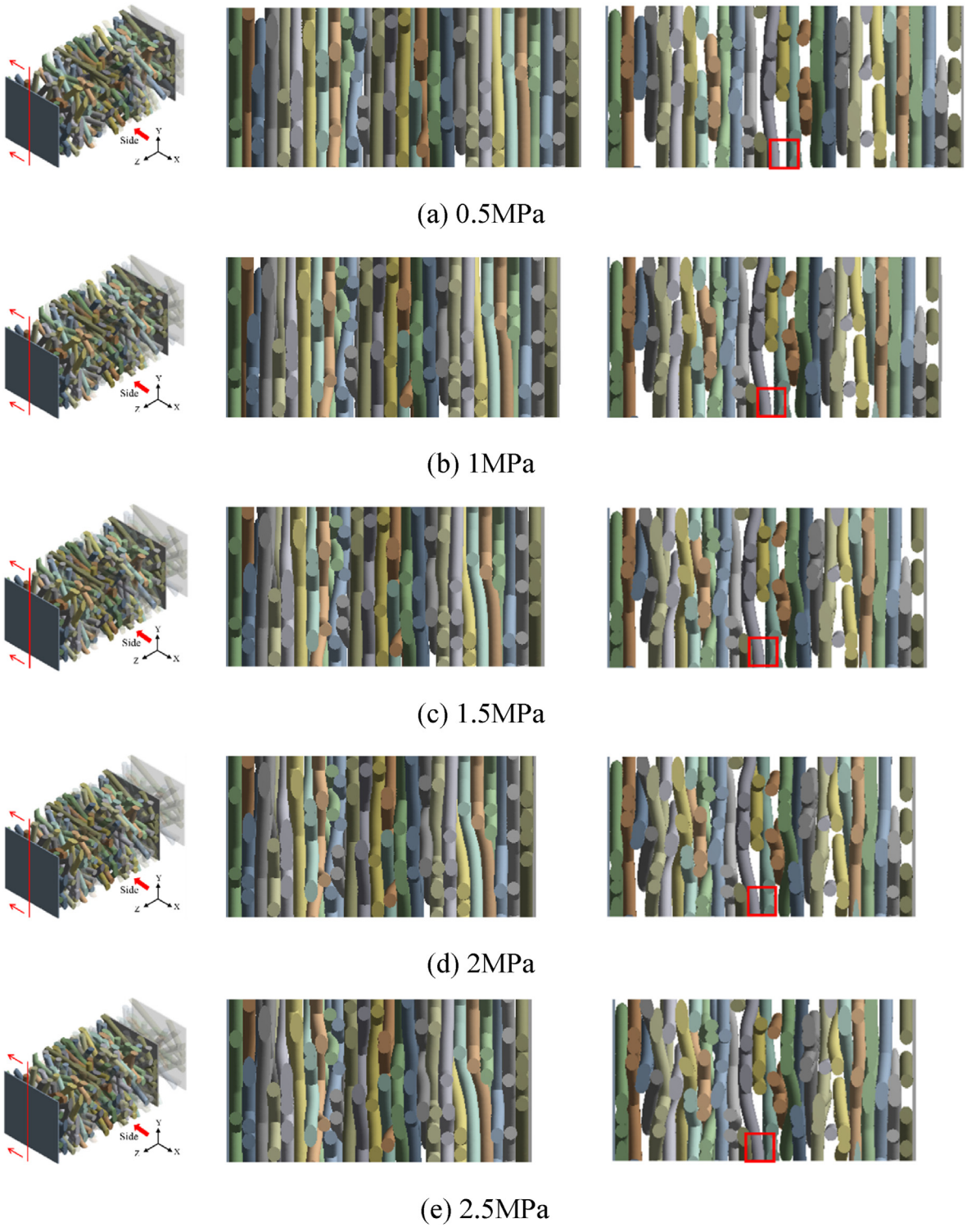

Fig. 7 – Compressed carbon paper of Case 1 under the different pressure in isometric view (left), side view, and section view (right).

other, increasing the resistance of compression and making carbon fiber difficult to deform. This is the reason why carbon paper presents nonlinear character of deformation, or why the equivalent Young's modulus of carbon paper increases with the increase of stress.

Fig. 8 shows the compressed carbon paper of different cases (Cases 2 to 7) under the pressure of 2.5 MPa. Similar compression processes from 0.5 MPa to 2.5 MPa for Cases 2 to 7 have been simulated, and they will not be repeated here for simplicity.

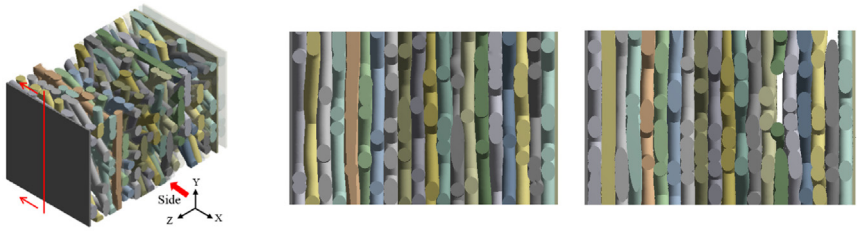

(a) Case 2 ϕ =58%

(b) Case 3 ϕ =68%

(c) Case 4 ϕ =73%

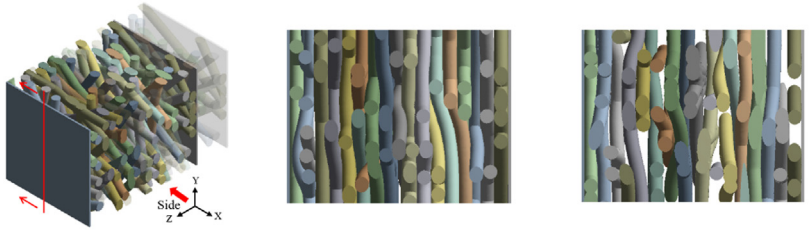

(d) Case 5 ϕ =78%

(e) Case 6 D=8μm

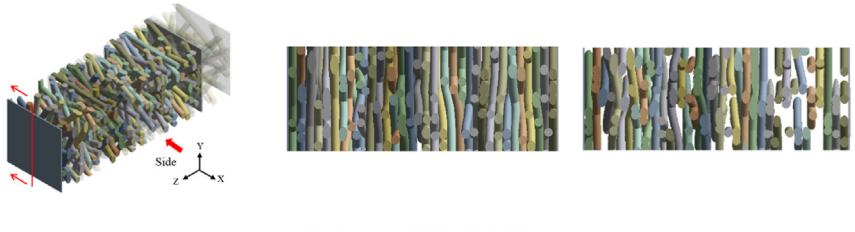

(f) Case 7 TGP-H-120

Fig. 8 – Compressed carbon paper of Cases 2 to 7 under 2.5 MPa stress in isometric view, side view and section view.

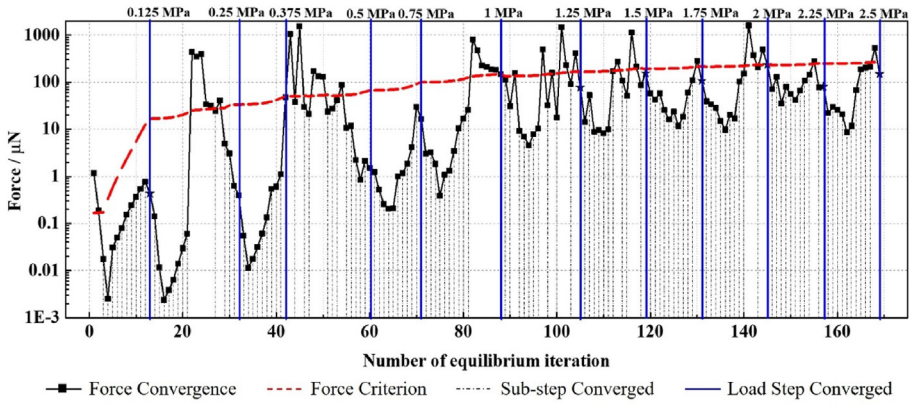

Fig. 9 – Force convergence curve of Case 1.

Solution procedure reflecting nonlinearity

In this section, the nonlinearity caused by the CAC contact is discussed from the FEM solution process. It is well-known that the change in contact state will lead to an abrupt change in the global stiffness matrix. For the convenience of convergence, a load step is better to be divided into several sub-steps, and within a sub-step solution, an iterative procedure (equilibrium iterations) is carried out to satisfy the specified convergence criterion. In the present static structure analysis, we choose force convergence as the convergence criterion. The force criterion value is equal to the product of absolute force value and relative tolerance value. The absolute force value is the square root of the sum of the squares (SRSS) of the applied loads, and the tolerance value is set to a constant 0.5%. As the number of iterations increases, the applied load of each sub-step increases, which causes an increase in the absolute value of the force convergence criterion. Take the first sub-step calculation of 0.125 MPa load step, for example, the convergence criteria in this sub-step is about 0.17 μN, and this sub-step converges after the completion of the third iteration.

As shown in Fig. 9, the distance between two adjacent dash-dotted lines is proportional to the number of iterations required to achieve the corresponding sub-step convergence. And more iterations reflect the increase of nonlinearity caused by the change of contact state in the current sub-step, from which we can further understand the nonlinear characteristics in the solution process.

Effect of three parameters on the stress-strain relation

Porosity

In order to study the effect of porosity on the stress-strain law of carbon paper, the compression processes for four porosities of 58%, 68%, 73%, and 78% were studied with other parameters such as fiber diameter and thickness being the same. Cases 2, 3, 4 and 5 in Table 4 represent the four situations. The predicted results in terms of stress vs. strain curves are presented in Fig. 10(a).

From Fig. 10(a), we can see that when the porosity of carbon paper is low, such as $\varphi = 58\%$ (Case 2) and $\varphi = 68\%$ (Case 3), the stress-strain curve of carbon paper is almost linear and shows a strong compression resistance. Compared with Case 2, the porosity of Case 3 is increased by ten points of percentage, its slope of the curve does not decrease too much, or Young's modulus does not decrease too much. Obviously, carbon paper of low porosity has less internal pores and a more compact structure, as shown in Figs. 8(a) and (b). In such cases, the compression mostly depends on the intrinsic elastic deformation of carbon fiber, and the effect of the pore in carbon paper is small. In addition, Young's modulus (hence the equivalent Young's modulus) of carbon fiber is as high as 3 GPa. These are the reasons why low porosity cases present a linear variation of stress vs. strain with a high slope.

When the porosity increases from 68% to 78% (Case 5) at the interval of 5%, the curve slopes of Case 4 and Case 5 are significantly reduced. For every 5% increase in porosity, the strain value increases by about 0.08 at 2.5 MPa. Increasing pore influence can explain this. In the carbon paper of larger porosity, the number of contacting pairs of fiber decreases, as shown in Figs. 8(c) and (d). Larger porosity and fewer contact pairs make deformation easier.

Fiber diameter

The carbon fiber diameter in GDL may vary from 6 to 10 μm [21,59–61]. In order to study the influence of fiber diameter on the stress-strain law of carbon paper, two fiber diameters are studied, 8 μm in Case 6 and 9.75 μm for all other cases, as shown in Table 4. The deformed carbon paper model of Case 5 and Case 6 are shown in Figs. 8(d) and (e), respectively. Under the same pressure, the more compact microstructure could be observed in Case 6 from the side and section view. The stress-strain curves of the two cases in Fig. 10(b) show that the carbon paper made of thinner carbon fiber is hard to deform. With the same porosity and carbon paper thickness, in the thinner fiber GDL, there are more layers of carbon fiber, and the number of carbon fibers in each layer also increases. As a result, the contacting fibers increases, and the deformation resistance increases. Therefore, the equivalent Young's modulus of carbon paper with smaller fiber diameter is larger than that of the bigger one.

Thickness

The Toray series carbon paper commonly used as GDL in PEMFC includes TGP-H-060, TGP-H-090, and TGP-H-120, with a nominal thickness of 190 μm, 280 μm, and 370 μm, respectively

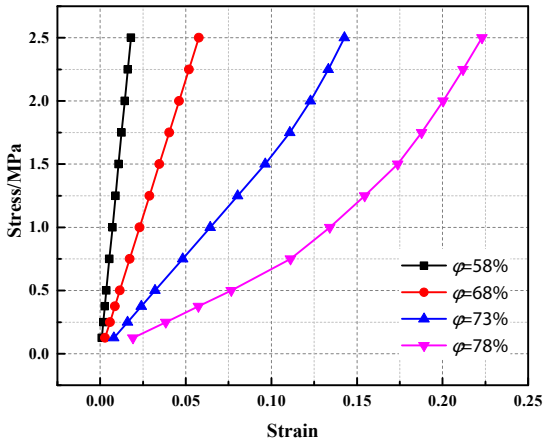

(a) The compressive curves of different porosity cases

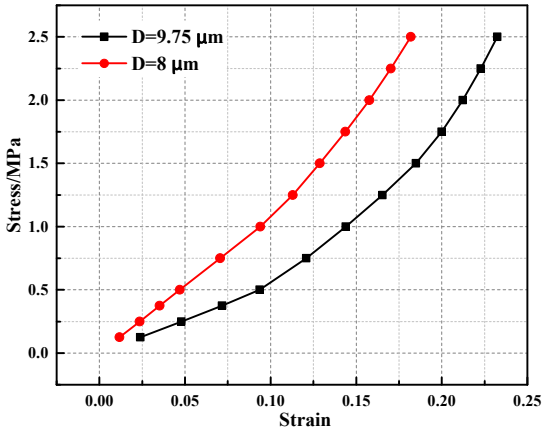

(b) The compressive curves of different fiber diameter cases

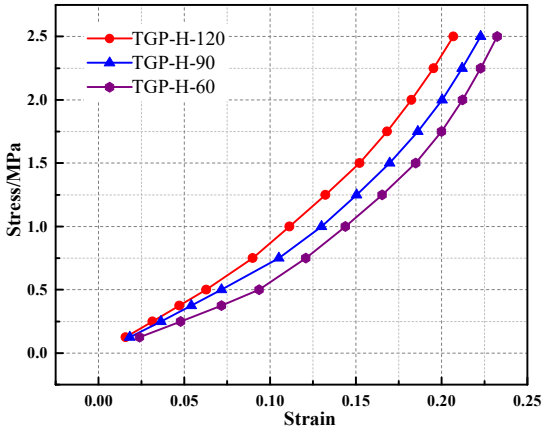

(c) The compressive curves of different thickness cases

Fig. 10 – Compressive curves of different cases.

[62]. Here, the effect of thickness on the stress-strain law is conducted for the three thickness values, and Cases 1, 5, 7 in Table 4 are the corresponding carbon paper, respectively. The stress-strain curves of the three cases are shown in Fig. 10(c). It can be found that the three curves are quite close to each other, which means the effect of thickness is relatively small compared with fiber diameter and porosity. Similarly, we focus on the pore space and contact pairs inside the carbon paper to explain this phenomenon. Under the same porosity, there is no difference in pore space percentage in the 3 cases, as shown in the isometric view in Figs. 7 and 8 (d) and (f). However, the absolute value of pore volume will increase, considering the increased total volume, and it causes a decrease of the deform resistance. On the other hand, with more layers, the number of contact pairs will increase (assuming that the contact pairs between each layer are approximately equal). Under these two opposite effects, the balanced results show that the influence of thickness is relatively small for the three cases studied.

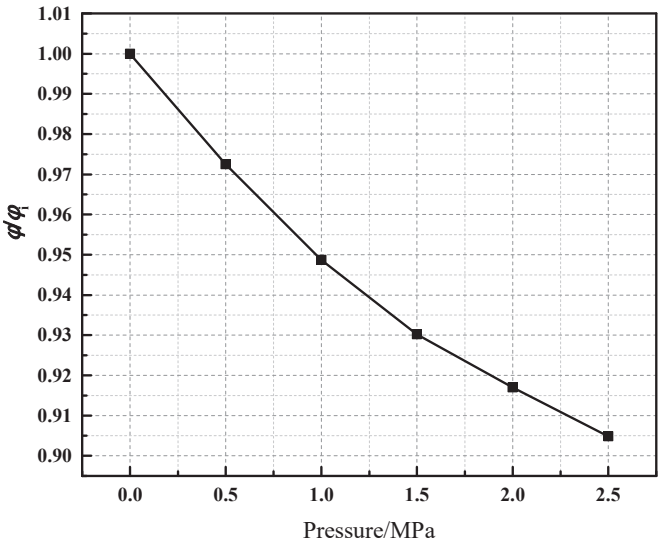

Fig. 11 – Porosity change with the pressure of Case 6.

Effects of compression on porosity

Porosity is a critical parameter that influences the performance of PEMFC. To study the porosity change under different pressure conditions, here we take Case 6, for example. The evolution of the integral porosity of the whole domain with pressure is shown in Fig. 11, where the ordinate takes the ratio of the porosity under pressure over its initial value. It can be seen that with the increase of pressure, the porosity of GDL decreases correspondingly, which is unfavorable for mass transfer. Like the stress-strain curve, it also shows a nonlinear change relationship. When the stress increases, the deformation is difficult, and the rate of porosity reduction slows down.

Figs. 12(a)–(f) show the local porosity distribution along the thickness direction at initial and the pressure of 0.5 MPa, 1 MPa, 1.5 MPa, 2 MPa, and 2.5 MPa respectively. In the figure, the dimensionless z-coordinate is normalized by the total thickness value. The total thickness of carbon paper is divided into 20 sections, and the local porosity of each section is calculated. The red dash line in each figure represents the integral porosity value under different pressure. From Figs. 12(a)–(f), we can find that the local porosity variation curve fluctuates up and down the average value line, and exhibits a

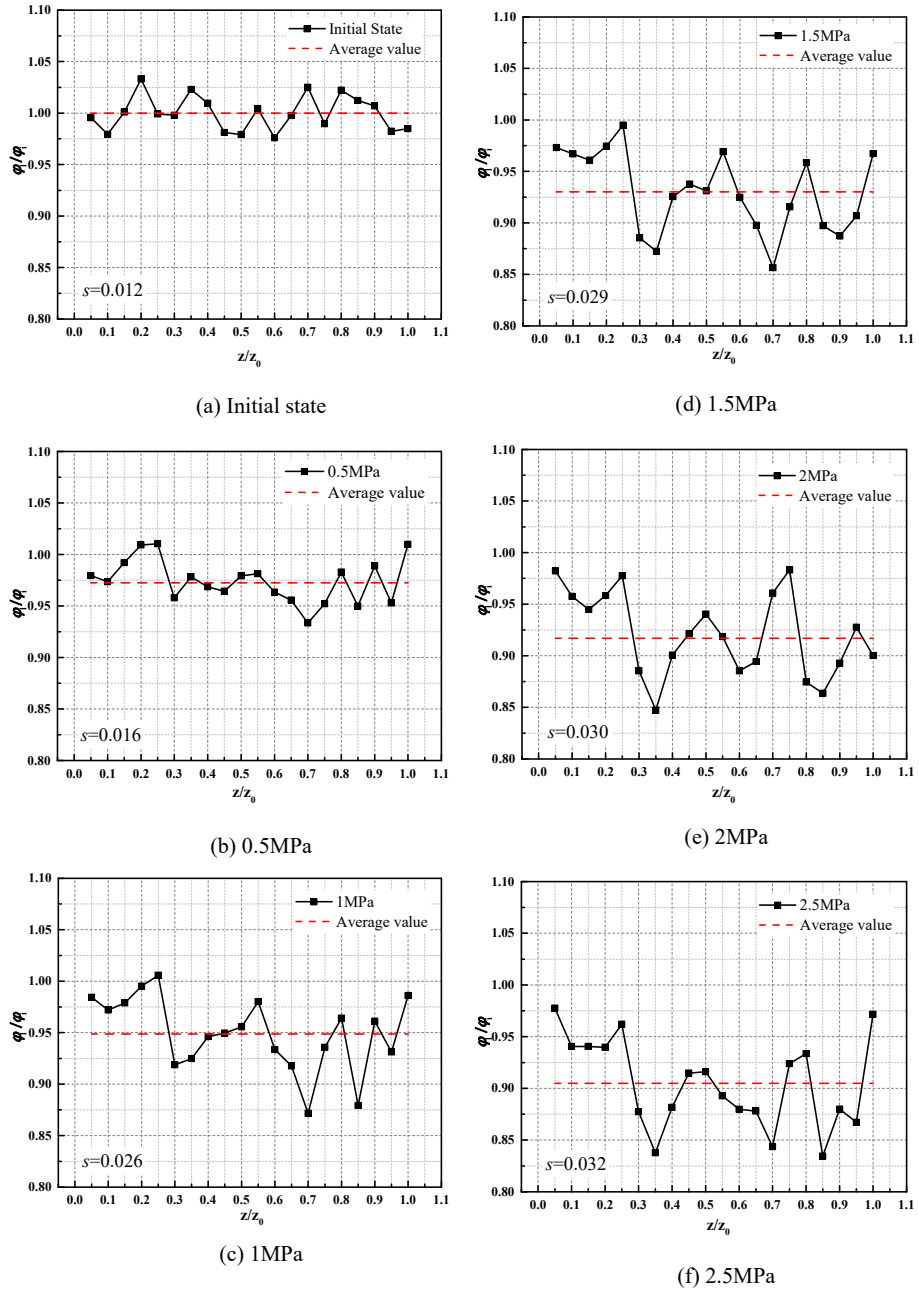

Fig. 12 – Local porosity distribution at initial and different pressure.

trend of downward movement or porosity decreasing with the increase in applied pressure. To quantitatively evaluate the fluctuation of the local porosity distribution curve, the standard deviation s is calculated and marked in the figure. With the increase of pressure, the standard deviation becomes larger, which represents an increase in porosity nonuniformity.

From the porosity distribution characteristics obtained above, we can infer that the PEMFC stack performance will be affected under the assembly pressure, which will be discussed in subsection Effects of compression on cell performance. Besides, the whole GDL region under high pressure cannot be characterized as a uniform porosity value, and more accurate porosity input is needed in the macro CFD model.

Effects of compression on cell performance

The GDL's compression under assembly pressure not only has an influence on its porosity but also affects its permeability, effective diffusivity, thermal conductivity, conductivity, and even liquid water transport. All these factors may directly affect transport phenomena in PEMFC. Therefore, further work will be required to investigate the effect of them on cell performance in detail.

However, based on the microstructure findings in the present study, here, a qualitative analysis of the effect of compression on ohmic loss and concentration loss of PEMFC is presented.

It is evident that there exists a suitable range of clamping pressure, which can balance mass transport and electric resistance in the GDL zone and achieve maximum stack power output [2,38]. These two aspects are related to the concentration loss and ohmic loss of cell performance. From the microscopic view, the deterioration of mass transfer in GDL under assembly pressure can be explained by the decrease of pores, as described in subsection Nonlinear deformation. According to the widely used effective gas diffusivity correlation Eq. (8) [24,30–35]:

$$D_j^{\text{eff}} = D_j \varphi^{1.5} \tag{8}$$

the effective diffusivity decreases, or in other words, gas diffusion in GDL weakened a lot. This means that the GDL's compression leads to a decrease of concentration to CL. In addition, the decrease of pore space slows down the discharge rate of liquid water, and may lead to higher flooding levels [28]. About the reduction of electrical resistance under assembly pressure, it can be explained by the increase of contact points, as also described in subsection Nonlinear deformation. During the compression process, the originally separated fibers come into contact, resulting in an additional contact area and lower resistance. And also, this is true for the fibers close to the endplate. The more contact points between fibers and endplate mean the lower contact resistance between BPP and GDL in practical. Both the electrical resistance of GDL itself and the electrical contact resistance between BPP and GDL decrease, which means the reduction of ohmic loss.

Conclusions

In the present study, the mechanical behavior of carbon paper used as GDL has been studied from a microscopic view. Through the FEM analysis based on the microstructure of carbon paper, the essential feature of carbon paper deformation has been revealed. The main findings of this study are as follows.

(1) For the simulation of the compression process of carbon paper, contact settings are important for both initial contacts (called Bond in this paper) and for the subsequent contact of carbon fiber pairs (called CAC) after deformation.
(2) The compressive curve of carbon paper shows nonlinear character, which is determined by its fibrous layered structure. Contact pairs and pore space of microstructure are two key factors determining the compressibility. More contact pairs and less pore space increase the difficulty to deform, leading to nonlinearity in the stress-strain relationship.
(3) Different porosity, fiber diameter, and thickness lead to different microstructure, and they all affect the carbon paper's deformation. The equivalent Young's modulus increases with the decrease of porosity and carbon fiber diameter, but it is not very sensitive to the carbon paper thickness.
(4) With the increase in acting pressure, the local porosity variation curve exhibits a trend of downward movement or porosity decreasing. Moreover, the degree of nonuniform distribution of porosity along through-plane direction increases.

Declaration of competing interest

The authors declare that they have no known competing financial interests or personal relationships that could have appeared to influence the work reported in this paper.

Acknowledgments

This work was supported by the Key Project of NNSFC (51836005), the National Key Research and Development Program (2017YFB0102702), the International Exchange Cooperation Project of NSFC-STINT (Energy Management of Fuel Cell Powered Data Centers) (51911530157), the Foundation for Innovative Research Groups of the National Natural Science Foundation of China (No.51721004), The Basic Research Project of Shaanxi Province (2019ZDXM3-01), the Key Science and Technology Project in Henan Province (Innovation Leading Project: 191110210200) and 111 Porject (B16038). The authors would like to thank Mr. Fan Bai and Le Lei for fruitful discussions.

REFERENCES

[1] Zhao J, Li X. A review of polymer electrolyte membrane fuel cell durability for vehicular applications: degradation modes and experimental techniques. Energy Convers Manag 2019;199:112022.
[2] Millichamp J, Mason TJ, Neville TP, Rajalakshmi N, Jervis R, Shearing PR, Brett DJL. Mechanisms and effects of mechanical compression and dimensional change in polymer electrolyte fuel cells – a review. J Power Sources 2015;284:305–20.
[3] Khetabi EM, Bouziane K, Zamel N, François X, Meyer Y, Candusso D. Effects of mechanical compression on the performance of polymer electrolyte fuel cells and analysis through in-situ characterisation techniques - a review. J Power Sources 2019;424:8–26.
[4] Mathias MF, Roth J, Fleming J, Lehnert W. Diffusion media materials and characterisation. In: Vielstich W, Lamm A, Gasteiger H, editiors, editors. Handbook of fuel cells. London: J. Wiley & Sons; 2003. p. 517–37.
[5] Shojaeefard MH, Molaeimanesh GR, Nazemian M, Moqaddari MR. A review on microstructure reconstruction of PEM fuel cells porous electrodes for pore scale simulation. Int J Hydrogen Energy 2016;41:20276–93.
[6] Qiu D, Janßen H, Peng L, Irmscher P, Lai X, Lehnert W. Electrical resistance and microstructure of typical gas diffusion layers for proton exchange membrane fuel cell under compression. Appl Energy 2018;231:127–37.

[7] Qiu D, Peng L, Yi P, Lai X. A micro contact model for electrical contact resistance prediction between roughness surface and carbon fiber paper. Int J Mech Sci 2017;124–125:37–47.
[8] Norouzifard V, Bahrami M. Deformation of PEM fuel cell gas diffusion layers under compressive loading: an analytical approach. J Power Sources 2014;264:92–9.
[9] Dafalla AM, Jiang F. Stresses and their impacts on proton exchange membrane fuel cells: a review. Int J Hydrogen Energy 2018;43:2327–48.
[10] Ge J, Higer A, Liu H. Effect og gas diffusion layer compression onPEM fuel cell performance. J Power Sources 2006;159:922–7.
[11] Baik KD, Hong BK, Han K, Kim MS. Correlation between anisotropic bending stiffness of GDL and land/channel width ratio of polymer electrolyte membrane fuel cells. Int J Hydrogen Energy 2012;37:11921–33.
[12] Carral C, Mélé P. A constitutive law to predict the compression of gas diffusion layers. Int J Hydrogen Energy 2018;43:19721–9.
[13] Escribano S, Blachot J-F, Ethève J, Morin A, Mosdale R. Characterization of PEMFCs gas diffusion layers properties. J Power Sources 2006;156:8–13.
[14] Ismail MS, Hassanpour A, Ingham DB, Ma L, Pourkashanian M. On the compressibility of gas diffusion layers in proton exchange membrane fuel cells. Fuel Cell 2012;12:391–7.
[15] Mason TJ, Millichamp J, Neville TP, El-kharouf A, Pollet BG, Brett DJL. Effect of clamping pressure on ohmic resistance and compression of gas diffusion layers for polymer electrolyte fuel cells. J Power Sources 2012;219:52–9.
[16] Nitta I, Hottinen T, Himanen O, Mikkola M. Inhomogeneous compression of PEMFC gas diffusion layer. J Power Sources 2007;171:26–36.
[17] Radhakrishnan V, Haridoss P. Effect of cyclic compression on structure and properties of a Gas Diffusion Layer used in PEM fuel cells. Int J Hydrogen Energy 2010;35:11107–18.
[18] Sadeghi E, Djilali N, Bahrami M. Effective thermal conductivity and thermal contact resistance of gas diffusion layers in proton exchange membrane fuel cells. Part 1: effect of compressive load. J Power Sources 2011;196:246–54.
[19] Saha LK, Tabe Y, Oshima N. Effect of GDL deformation on the pressure drop of polymer electrolyte fuel cell separator channel. J Power Sources 2012;202:100–7.
[20] Radhakrishnan V, Haridoss P. Differences in structure and property of carbon paper and carbon cloth diffusion media and their impact on proton exchange membrane fuel cell flow field design. Mater Des 2011;32:861–8.
[21] Bazylak A, Sinton D, Liu ZS, Djilali N. Effect of compression on liquid water transport and microstructure of PEMFC gas diffusion layers. J Power Sources 2007;163:784–92.
[22] Roy Chowdhury P, Vikram A, Phillips RK, Hoorfar M. Measurement of effective bulk and contact resistance of gas diffusion layer under inhomogeneous compression – Part II: thermal conductivity. J Power Sources 2016;320:222–30.
[23] Froning D, Yu J, Gaiselmann G, Reimer U, Manke I, Schmidt V, Lehnert W. Impact of compression on gas transport in non-woven gas diffusion layers of high temperature polymer electrolyte fuel cells. J Power Sources 2016;318:26–34.
[24] Zhou Y, Jiao K, Du Q, Yin Y, Li X. Gas diffusion layer deformation and its effect on the transport characteristics and performance of proton exchange membrane fuel cell. Int J Hydrogen Energy 2013;38:12891–903.
[25] Carral C, Mélé P. A numerical analysis of PEMFC stack assembly through a 3D finite element model. Int J Hydrogen Energy 2014;39:4516–30.
[26] Chien C-H, Hu Y-L, Su T-H, Liu H-T, Wang C-T, Yang P-F, Lu Y-X. Effects of bolt pre-loading variations on performance of GDL in a bolted PEMFC by 3-D FEM analysis. Energy 2016;113:1174–87.
[27] Liang P, Qiu D, Peng L, Yi P, Lai X, Ni J. Contact resistance prediction of proton exchange membrane fuel cell considering fabrication characteristics of metallic bipolar plates. Energy Convers Manag 2018;169:334–44.
[28] Mahmoudi AH, Ramiar A, Esmaili Q. Effect of inhomogeneous compression of gas diffusion layer on the performance of PEMFC with interdigitated flow field. Energy Convers Manag 2016;110:78–89.
[29] Hottinen T, Himanen O, Karvonen S, Nitta I. Inhomogeneous compression of PEMFC gas diffusion layer. J Power Sources 2007;171:113–21.
[30] Xu Y, Qiu D, Yi P, Lan S, Peng L. An integrated model of the water transport in nonuniform compressed gas diffusion layers for PEMFC. Int J Hydrogen Energy 2019;44:13777–85.
[31] Toghyani S, Moradi Nafchi F, Afshari E, Hasanpour K, Baniasadi E, Atyabi SA. Thermal and electrochemical performance analysis of a proton exchange membrane fuel cell under assembly pressure on gas diffusion layer. Int J Hydrogen Energy 2018;43:4534–45.
[32] Movahedi M, Ramiar A, Ranjber AA. 3D numerical investigation of clamping pressure effect on the performance of proton exchange membrane fuel cell with interdigitated flow field. Energy 2018;142:617–32.
[33] Li WZ, Yang WW, Zhang WY, Qu ZG, He YL. Three-dimensional modeling of a PEMFC with serpentine flow field incorporating the impacts of electrode inhomogeneous compression deformation. Int J Hydrogen Energy 2019;44:22194–209.
[34] Li S, Sundén B. Effects of gas diffusion layer deformation on the transport phenomena and performance of PEM fuel cells with interdigitated flow fields. Int J Hydrogen Energy 2018;43:16279–92.
[35] Atyabi SA, Afshari E, Wongwises S, Yan W-M, Hadjadj A, Shadloo MS. Effects of assembly pressure on PEM fuel cell performance by taking into accounts electrical and thermal contact resistances. Energy 2019;179:490–501.
[36] Lu Z, Kim C, Karlsson AM, Cross JC, Santare MH. Effect of gas diffusion layer modulus and land–groove geometry on membrane stresses in proton exchange membrane fuel cells. J Power Sources 2011;196:4646–54.
[37] Kleemann J, Finsterwalder F, Tillmetz W. Characterisation of mechanical behaviour and coupled electrical properties of polymer electrolyte membrane fuel cell gas diffusion layers. J Power Sources 2009;190:92–102.
[38] Yan X, Lin C, Zheng Z, Chen J, Wei G, Zhang J. Effect of clamping pressure on liquid-cooled PEMFC stack performance considering inhomogeneous gas diffusion layer compression. Appl Energy 2020;258:114073.
[39] Serincan MF, Pasaogullari U. Effect of gas diffusion layer anisotropy on mechanical stresses in a polymer electrolyte membrane. J Power Sources 2011;196:1314–20.
[40] García-Salaberri PA, Vera M, Zaera R. Nonlinear orthotropic model of the inhomogeneous assembly compression of PEM fuel cell gas diffusion layers. Int J Hydrogen Energy 2011;36:11856–70.
[41] Gigos PA, Faydi Y, Meyer Y. Mechanical characterization and analytical modeling of gas diffusion layers under cyclic compression. Int J Hydrogen Energy 2015;40:5958–65.
[42] Yi P, Peng L, Lai X, Ni J. A numerical model for predicting gas diffusion layer failure in proton exchange membrane fuel cells. J Fuel Cell Sci Technol 2010;8.
[43] Toll S. Packing mechanics of fiber reinforcements. Polym Eng Sci 1998;38:1337–50.
[44] Rodney D, Fivel M, Dendievel R. Discrete modeling of the mechanics of entangled materials. Phys Rev Lett 2005;95:108004.

[45] Barbier C, Dendievel R, Rodney D. Role of friction in the mechanics of nonbonded fibrous materials. Phys Rev 2009;80. 016115.
[46] Xiao L, Luo M, Zhang H, Zeis R, Sui P-C. Solid mechanics simulation of reconstructed gas diffusion layers for PEMFCs. J Electrochem Soc 2019;166:F377–85.
[47] Zhou X, Niu Z, Li Y, Sun X, Du Q, Xuan J, Jiao K. Investigation of two-phase flow in the compressed gas diffusion layer microstructures. Int J Hydrogen Energy 2019;44:26498–516.
[48] Zhou X, Niu Z, Bao Z, Wang J, Liu Z, Yin Y, Du Q, Jiao K. Two-phase flow in compressed gas diffusion layer: finite element and volume of fluid modeling. J Power Sources 2019;437:226933.
[49] Zamel N, Li X, Shen J. Correlation for the effective gas diffusion coefficient in carbon paper diffusion media. Energy Fuel 2009;23:6070–8.
[50] Daino MM, Kandlikar SG. 3D phase-differentiated GDL microstructure generation with binder and PTFE distributions. Int J Hydrogen Energy 2012;37:5180–9.
[51] Hao L, Cheng P. Pore-scale simulations on relative permeabilities of porous media by lattice Boltzmann method. Int J Heat Mass Tran 2010;53:1908–13.
[52] Mukherjee PP, Kang Q, Wang CY. Pore-scale modeling of two-phase transport in polymer electrolyte fuel cells—progress and perspective. Energy Environ Sci 2011;4.
[53] Chen L, Luan H-B, He Y-L, Tao W-Q. Pore-scale flow and mass transport in gas diffusion layer of proton exchange membrane fuel cell with interdigitated flow fields. Int J Therm Sci 2012;51:132–44.
[54] Schulz VP, Becker Jr, Wiegmann A, Mukherjee PP, Wang C-Y. Modeling of two-phase behavior in the gas diffusion medium of PEFCs via full morphology approach. J Electrochem Soc 2007;154:B419.
[55] Inoue G, Yoshimoto T, Matsukuma Y, Minemoto M. Development of simulated gas diffusion layer of polymer electrolyte fuel cells and evaluation of its structure. J Power Sources 2008;175:145–58.
[56] Schladitz K, Peters S, Reinel-Bitzer D, Wiegmann A, Ohser J. Design of acoustic trim based on geometric modeling and flow simulation for non-woven. Comput Mater Sci 2006;38:56–66.
[57] Fadzillah DM, Rosli MI, Talib MZM, Kamarudin SK, Daud WRW. Review on microstructure modelling of a gas diffusion layer for proton exchange membrane fuel cells. Renew Sustain Energy Rev 2017;77:1001–9.
[58] Naito K, Tanaka Y, Yang J-M. Transverse compressive properties of polyacrylonitrile (PAN)-based and pitch-based single carbon fibers. Carbon 2017;118:168–83.
[59] Gao Y, Hou Z, Wu X, Xu P. The impact of sample size on transport properties of carbon-paper and carbon-cloth GDLs: direct simulation using the lattice Boltzmann model. Int J Heat Mass Tran 2018;118:1325–39.
[60] Holzer L, Pecho O, Schumacher J, Marmet P, Stenzel O, Büchi FN, Lamibrac A, Münch B. Microstructure-property relationships in a gas diffusion layer (GDL) for Polymer Electrolyte Fuel Cells, Part I: effect of compression and anisotropy of dry GDL. Electrochim Acta 2017;227:419–34.
[61] Hinebaugh J, Bazylak A. Stochastic modeling of polymer electrolyte membrane fuel cell gas diffusion layers – Part 1: physical characterization. Int J Hydrogen Energy 2017;42:15861–71.
[62] Toray carbon paper specification sheet. Tokyo: Toray Industries Inc.; 2011 (revised May 16th).